

## Continuum mechanics of crack blunting on the atomic scale: elastic solutions

Lisa L Fischer and Glenn E Beltz

Department of Mechanical and Environmental Engineering, University of California, Santa Barbara, CA 93106, USA

Received 14 November 1996, accepted for publication 25 June 1997

**Abstract.** In order to improve upon continuum models for understanding the origins of ductile versus brittle response in materials, an accurate assessment of the stress fields near a crack tip must be developed. Existing continuum models have considered the crack tip to be perfectly sharp in order to use convenient analytical solutions for the stress fields around the crack tip. Numerous experimental observations have indicated that an atomically sharp crack is very rare and that crack tip blunting can precede or accompany crack propagation. A two-dimensional finite element model has been developed to evaluate the stress fields at a blunted crack tip subjected to loading. Stress fields have been calculated for mode I loading as well as for the self-stress due to the presence of a dislocation near a crack tip. These calculated stress fields have been compared with analytical solutions for appropriate limiting cases.

### 1. Introduction

A theoretical understanding of the ductile versus brittle behavior of a material is generally understood in terms of a competition between crack propagation and material relaxation mechanisms. Ductile fracture is associated with ease of dislocation nucleation as well as ease of dislocation motion on activated slip planes which can be a precursor for crack propagation through void growth ahead of the crack tip. Brittle fracture, on the other hand, is associated with very little dislocation mobility (as in the case of materials like silicon below its brittle–ductile transition temperature) or atomically sharp crack motion that persists when dislocations do not nucleate (possible in iron, embrittled metals, or even on metal–ceramic interfaces). For the past 20 to 30 years several methods have been proposed to predict whether a sharp crack tip will blunt, possibly leading to ductile failure, or continue to cleave in a brittle fashion.

This paper is the first in a series which explores the post-dislocation-emission behavior of a crack, in an attempt to understand if the nucleation of a single dislocation will *always* lead to a ductile response or if subsequent brittle propagation can occur. Here, a two-dimensional finite element model has been developed to evaluate the stress fields at a blunted crack tip subjected to loading. Since the model is two-dimensional, the analysis neglects the inherently three-dimensional aspects of thermally activated dislocation loop nucleation. The two types of loading studied will be of central importance in our future work. Stress fields have been calculated for far-field mode I loading and compared to an asymptotic field for a sharp crack. Stress fields have also been calculated for the presence of a dislocation near a blunted crack tip and compared to the stress fields resulting from the presence of a dislocation near a sharp crack tip. The purpose of this paper is to present

these separate classes of *elastic* solutions. In future work, these elastic solutions will provide kernel functions from which a framework for determining the fracture behavior of a blunted crack geometry under various loading will be built.

In general, two types of models have been developed to quantify crack tip behavior: continuum and atomistic. As an example of the former, the Rice–Thomson model [1] proposed that the competition between dislocation emission and atomic decohesion at the crack tip is the controlling factor in the ductile versus brittle behavior of a material. The Rice–Thomson model used the Griffith criterion for cleavage requirements and developed a quantitative evaluation of conditions for dislocation emission from the near-tip region. It was shown that the ratio  $\gamma/\mu b$  ( $\gamma$  = surface energy,  $\mu$  = shear modulus,  $b$  = Burgers vector) was a good indicator of the ductile versus brittle response. The Rice–Thomson model has evolved continuously, to account for elastic anisotropy, bimaterial interfaces, nonlinear dislocation core structures, and realistic slip system geometries. The latter phenomena are addressed in the recent work of Xu *et al* [2] and references therein. Despite repeated improvements made in later versions of the Rice–Thomson model and other studies of ductile versus brittle behavior, one assumption has typically been made: *crack tips are atomically sharp, and remain so during the dislocation nucleation event*. This is a fundamental assumption in the development of the analytical solution, thereby ruling out the study of initially blunt cracks.

The physical reality of a blunted crack configuration has motivated limited attempts at evaluating its effect and determining to what extent its stress fields differ from the sharp crack stress fields. Schiøtz [3,4] has tackled this problem using a conformal mapping technique. Using the Schwarz–Christoffel transformation, a simple  $60^\circ$  blunted crack tip can be mapped to the upper complex half plane with  $z = x_1 + ix_2$ . The stress fields for mode III loading can be solved using anti-plane elasticity and then the reverse mapping transformations can be made to find the mode III stress fields of the blunted crack tip. While this technique does give a concise analytical solution, it is too cumbersome to carry out for the more applicable case of in-plane loadings, which display stronger singular stress fields [5].

Mode I blunt crack configurations can, on the other hand, be studied atomistically because the only assumptions made in these models regard the nature of the interactions between the individual atoms. However, this process is extremely calculation intensive and expensive if one wants to study a configuration of reasonable size. Recent work done on atomistic models developed by Schiøtz and co-workers [3,4], Gumbsch and co-workers [6,7], and Thomson [8] have provided partial motivation for the development of the model and specific geometry discussed in this paper.

To complement the analytical solutions of the mode III stress fields of a blunted crack, Schiøtz *et al* [4] developed an atomistic model to study the effects of crack tip blunting on further crack propagation and dislocation emission. The simulations were carried out for mode I and mode II loading using a hexagonal two-dimensional atomistic model that consisted of two regions. In the region near the crack tip, the atoms interacted through a nonlinear force law. Further from the crack tip, the atoms interacted through linear forces described using a lattice Green's function developed earlier by Thomson [8]. The results of the simulations for mode I loading showed that crack blunting increased the required force to propagate the crack. For a blunting height of ten layers of atoms, there was an increase of 15 to 20% in the force required for propagation. For some materials, this could result in a change of behavior from crack propagation to dislocation emission.

The studies carried out by Gumbsch and co-workers [6,7] use a hybrid finite element–atomistic (FE–At) mesh comprising a limited atomistic core around the crack tip coupled

with an outer boundary of finite elements. Primarily, Gumbsch compared the energy requirements for brittle fracture of the 'FE-At' model with various continuum mechanics energy criteria and found good agreement with simple mode I-II loadings where the slip plane coincides with the crack plane. In these cases, dislocation nucleation does not result in blunting or ledge formation. In the cases where dislocation nucleation does result in blunting, the FE-At and continuum energy requirements diverge with increasing blunting height. Figure 1 shows some of the blunted geometries that were tested and their deviation from sharp crack solutions [7].

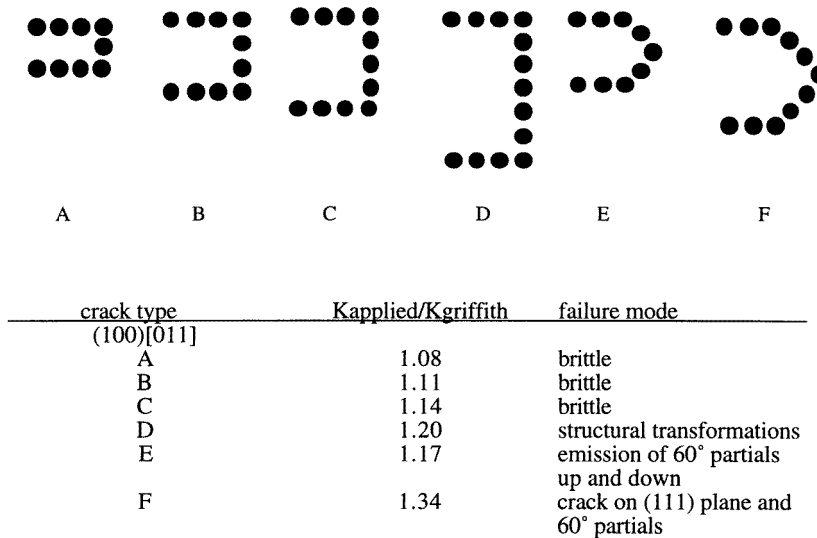


Figure 1. Gumbsch blunted geometry results [7].

Thomson [8] also studied cleavage versus blunting with a two-dimensional (2D) simple hexagonal lattice. The hexagonal lattice results in slip planes which intersect the crack front at a 60° angle. The geometry of the 2D simple hexagonal lattice dictates the geometry of the finite element model used here.

Upon reviewing current models for quantifying ductile versus brittle fracture behavior, the motivation for studying the stress fields in a blunted crack geometry becomes clear. Changes in the crack tip geometry will significantly affect the stress fields around the crack tip, which can change the favorability of crack advancement or dislocation emission. It is believed that this effect will make a significant contribution to a reconciliation between the predictions of continuum-based and atomistic-based models. The purpose of the present paper is to present a 2D finite element model using the program ABAQUS to determine the modified stress fields.

## 2. Model development

The mesh is based on a simple circular crack tip mesh. There are only three geometric parameters, shown in figure 2, that need to be specified: the height of the blunted notch,  $h$ , the size of the mesh,  $H$ , and the angle of the blunting slip plane,  $\alpha$ . Although no dislocation is involved in the mode I loading cases, the geometrical parameters are based on a burgers

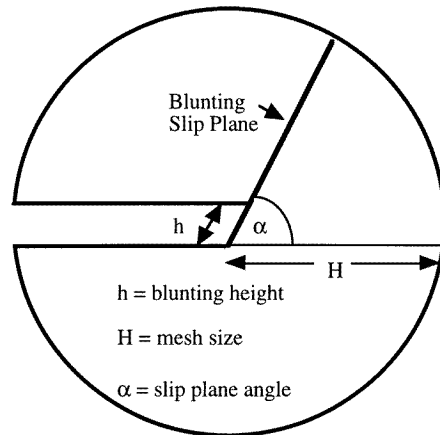


**Figure 2.** Diagram of mesh parameters.

vector,  $b$ . Given a unitless burgers vector of 4, the height of the blunting is 40, or simply ten times the burgers vector. Later, it will be clear from dimensional arguments that there is no loss of generality from choosing a single set of parameters.

The size, or average radius of the mesh, is one hundred times the burgers vector. This large size is motivated by the consideration that the mesh needs to be large enough to compare far-field solutions of blunted and sharp crack solutions. It is expected that the two solutions will converge as the distance from the crack tip increases. One hundred burgers vectors can be considered relatively far from the crack tip, because we are considering the regime involving a small number of emitted dislocations. The angle of the slip plane with respect to the crack plane is  $60^\circ$ . This angle was chosen in order to compare results with the concurrent studies of Schiøtz and co-workers and Thomson, which also make use of a  $60^\circ$  slip plane angle.

Initially, three different meshes were developed with the same basic geometry but with varying refinements and nodal positioning patterns [9]. The mesh which provided the smoothest, most consistent values of the stresses ahead of the crack tip, along the  $0^\circ$  line, and for the stresses in the slip plane ahead of the blunted corner, along the  $60^\circ$  line, was used for the final calculated stress fields. The mesh which produced the best results is shown in figure 3(a) and is referred to as the *gradual* mesh.

The gradual mesh is composed of 8410 four-node plane strain elements and a total of 144 eight-node plane strain elements near the two corners of the blunted tip. Using plane strain elements makes the assumption that the crack front is infinitely long in the third dimension such that the displacement in that direction vanishes. As seen in figure 3(a) the element sizes become smaller as they approach the crack tip. Near the crack tip the largest dimension of the elements is on the order of half a burgers vector. There exist means of creating elements that will display desired stress singularities about a crack tip. For example, for a sharp crack tip, the stress singularity is known analytically to vary as  $r^{-1/2}$ . Elements can be tailored to display a  $r^{-1/2}$  stress singularity simply by controlling nodal point coordinates [10]; such configurations are known as quarter-point elements. That is, one of the four sides of an eight-node quadrilateral element is collapsed such that the three nodes on that side share the same coordinates. Then, the nodes along the radially oriented sides are arranged such that the center nodes are one quarter the length of the side

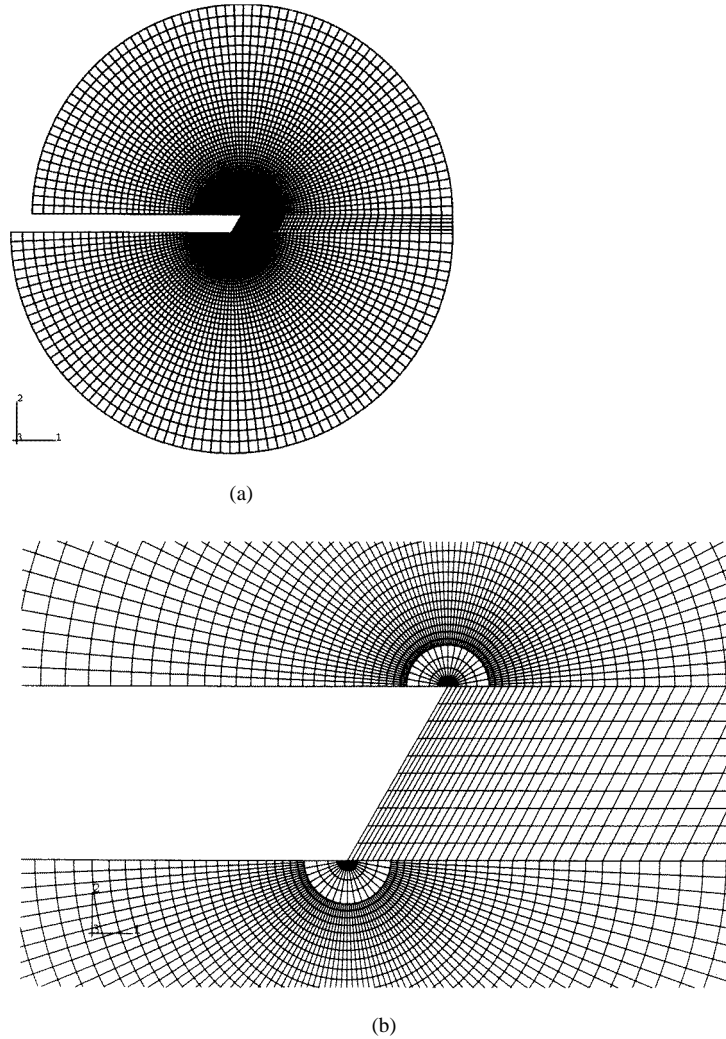


**Figure 3.** (a) Gradual finite element mesh. (b) Close up of gradual finite element mesh indicating angles of crack tip.

of the element from the collapsed side. However, this element development procedure is not absolutely necessary to obtain good results when mesh refinement has been carried out to the degree it is here.

### 3. Mode I loading

In order to subject the mesh to mode I loading, it is assumed that the far-field displacements of a sharp and blunted crack will converge. The displacement fields of a sharp crack under mode I loading are known and can be written in terms of the original radial and angular position measured from the crack tip. Here,  $u$  is the displacement in the  $x$  direction, and  $v$

is the displacement in the  $y$  direction [11].

$$u = \frac{K}{\mu} \sqrt{\frac{r}{2\pi}} \left( \cos \frac{\theta}{2} \right) \left( 2(1 - \nu) - \cos^2 \frac{\theta}{2} \right) \quad (1a)$$

$$v = \frac{K}{\mu} \sqrt{\frac{r}{2\pi}} \left( \sin \frac{\theta}{2} \right) \left( 2(1 - \nu) - \cos^2 \frac{\theta}{2} \right). \quad (1b)$$

For these displacement calculations,  $r$  is measured from the  $120^\circ$  crack tip and,  $\theta$  is measured from the horizontal just right of the  $120^\circ$  crack tip. The displacements are dependent upon the constants,  $\mu$ , the shear modulus,  $\nu$ , the Poisson's ratio, and  $K$ , the far-field mode I stress intensity factor which is a constant that only contains information about the magnitude of the *outer* loading and geometric details. Plane strain conditions are assumed; therefore the displacement in the  $z$  direction,  $w$ , vanishes. The major differences in the displacement fields for the sharp and blunted cracks will primarily occur close to the crack tip where the geometry differs significantly. The blunted mesh can then be loaded by applying the sharp crack displacements to the nodes at the outer edge which is approximately one hundred burgers vectors from the crack tip. The near tip stresses are then calculated.

### 3.1. Mode I results

Figure 4 shows the radial stress along the  $0^\circ$  line of the original three different meshes resulting from mode I loading. A complete collection of hoop, radial, and shear stresses for the  $0^\circ$  and  $60^\circ$  lines obtained from the gradual mesh are presented. As evidenced in figure 4, three meshes of varying degree of refinement provide similar results; but the smoothest results are given by the gradual mesh, which differ by less than 2% from the previous refinement step. Therefore, the results shown in figure 5 and the rest of this paper will be limited to that of the gradual mesh (figure 3(a)). The radial stresses along the  $0^\circ$  crack front and along the  $60^\circ$  slip plane are presented first. Then, the hoop stresses for the two different directions and finally the shears are presented.

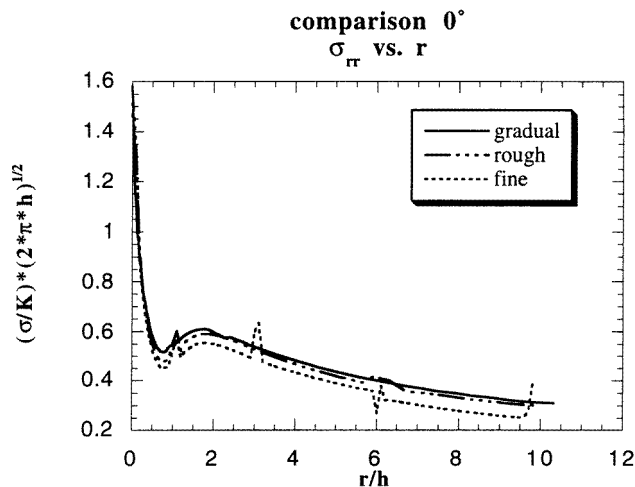


**Figure 4.** Mode I loading results for the radial stress along the crack front for three meshes. The rough and fine mesh were preliminary to the development of the gradual mesh which gives much smoother results.

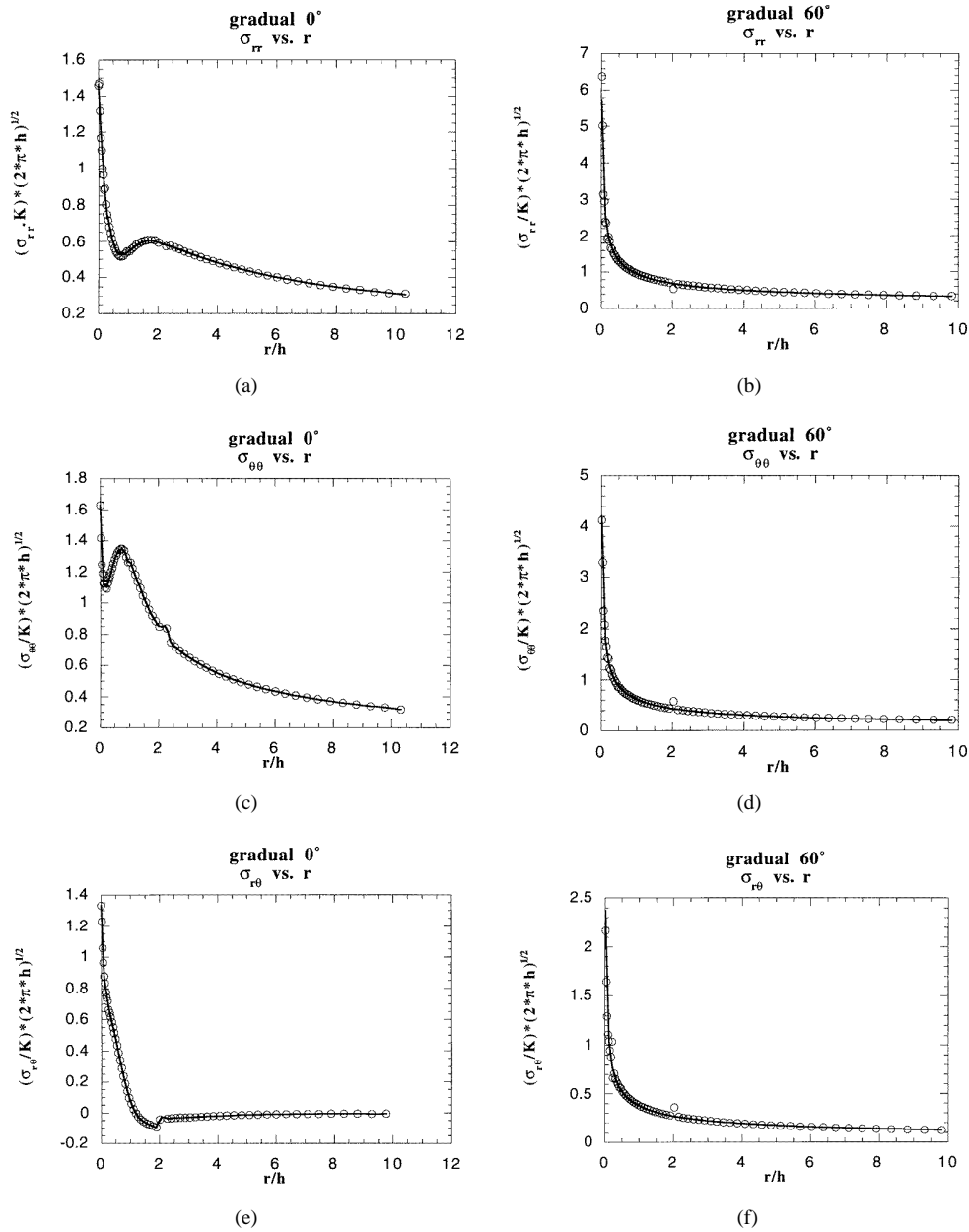


**Figure 5.** Mode I loading results from the gradual mesh (a) radial stress on the 0° crack front, (b) radial stress on the 60° slip plane, (c) hoop stress on the 0° crack front, (d) hoop stress on the 60° slip plane, (e) shear stress on the 0° crack front, and (f) shear stress on the 60° slip plane.

The distances from the crack tip or 60° corner,  $r$ , have been normalized by the blunting height,  $h$ . The stress values have been normalized by  $K/(2\pi h)^{1/2}$ , the only grouping of physical constants in this problem that result in units of stress. The appropriateness of this normalization has been highlighted in the earlier work of Hsia *et al* [12]. Exact data points

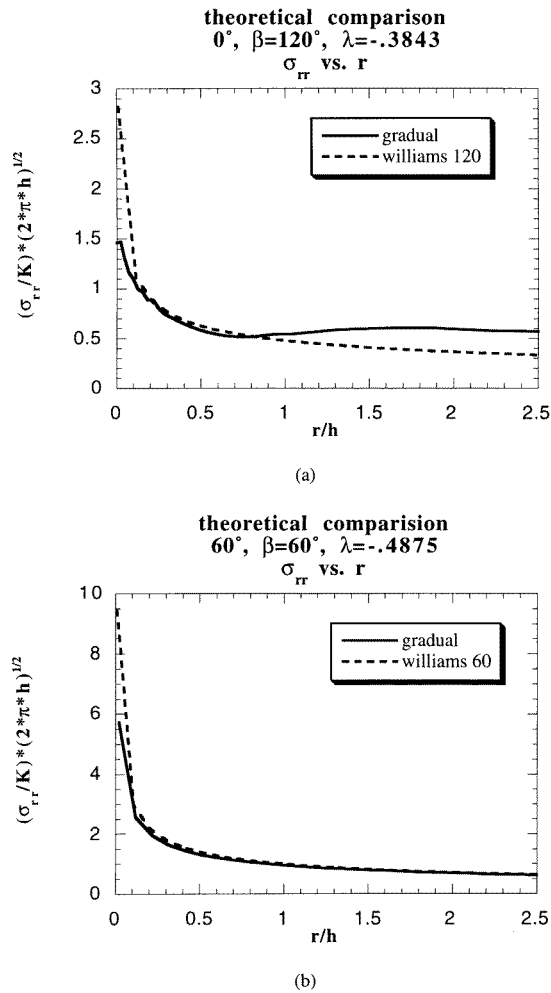


**Figure 6.** Comparison of the Williams asymptotic stress field with finite element results for (a) a wedge of  $120^\circ$  along the crack front, and (b) a wedge of  $60^\circ$  along the slip plane.

have been indicated with open circles and smooth curves have been interpolated for the data.

### 3.2. Williams comparison

Comparison of the results from the three different meshes provides a good check for their consistency, but a more rigorous comparison can be made with the work of Williams. Williams [5] developed a means of calculating the radial dependence of stress singularities for sharp wedges with an angle greater than  $0^\circ$ . In the blunted crack mesh, there are two singularities. As shown in figure 3(b), the actual crack tip has wedge angles of  $120^\circ$  and  $60^\circ$ . Near the crack tip and corner, the finite element results should approach the analytical results for sharp wedges. Stress fields around a sharp crack with an angle of  $0^\circ$  have an  $r^{-1/2}$  dependence. In appendix A it is shown that a wedge with an angle of  $120^\circ$  has

an  $r^{-0.3843}$  dependence and a wedge with an angle of  $60^\circ$  has an  $r^{-0.4875}$  dependence. Figure 6(a) compares the radial stress along the  $0^\circ$  line with the  $r^{-0.3843}$  dependence and figure 6(b) compares the radial stress along the  $60^\circ$  line with the  $r^{-0.4875}$  dependence. In both cases the finite element results near the crack tip and corner agree with the analytical radial dependence predicted by Williams.

#### 4. Dislocation near the crack tip

The ABAQUS finite element program does not provide a simple means of inserting a dislocation within a mesh. However, the principle of superposition can be used to obtain the stress fields of the blunted crack tip in the presence of a dislocation. When the stress field solutions for a dislocation in an infinite medium are added to the stress field solutions for a loading of opposite tractions along the crack boundary a traction free surface results at the blunted crack boundary. The calculations are carried out in three steps. First, the stress fields for a dislocation in an *infinite* continuum shown in figure 7 are calculated. The stress field expressions for a dislocation centered at the origin of the domain are given as [13]

$$\sigma_{xx} = \frac{-\mu b}{2\pi(1-\nu)} \frac{y(3x^2 + y^2)}{(x^2 + y^2)^2} \quad (2a)$$

$$\sigma_{yy} = \frac{\mu b}{2\pi(1-\nu)} \frac{y(x^2 - y^2)}{(x^2 + y^2)^2} \quad (2b)$$

$$\sigma_{xy} = \frac{\mu b}{2\pi(1-\nu)} \frac{x(x^2 - y^2)}{(x^2 + y^2)^2}. \quad (2c)$$

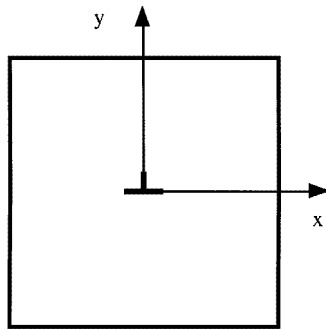
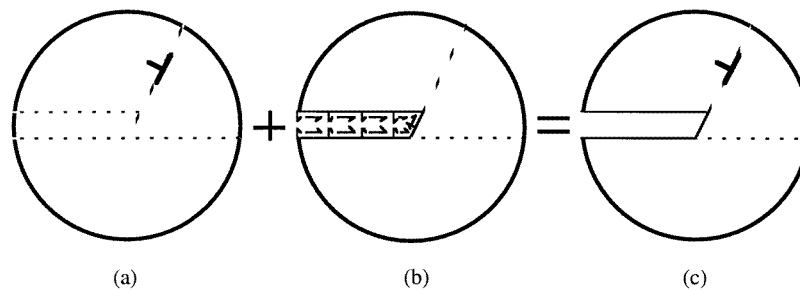


Figure 7. Edge dislocation in a continuum.

In this case, the stresses at the positions of the crack boundary, along the  $0^\circ$  line, and along the  $60^\circ$  line are calculated for some desired orientation of the dislocation with respect to the crack tip. Figure 8(a) shows the positions of the calculated stresses with dashed lines. Once these stresses have been calculated, the negative values of the normal tensions and shears for the crack boundary can be applied to the finite element model as shown in figure 8(b). It is necessary to pin the model at two points far from the crack tip to avoid rigid body modes in the finite element model results. Loading the finite element model along the crack boundary will result in a second stress field solution. When the stress fields for these two loadings are superimposed, the boundary of the crack becomes stress free, yielding the net result of the stress fields of a blunted crack tip in the presence of a dislocation. These calculations have been carried out for dislocations along the  $60^\circ$  line at

various distances from the crack tip and for dislocations vertically oriented along the  $0^\circ$  line at various distances from the crack tip. Figure 9 shows the two types of dislocation orientation that were studied.



**Figure 8.** The superposition of stress fields is illustrated with (a) the stresses of a dislocation in a continuum plus (b) the negative values of the normal tensions and shears for the crack boundary equaling (c) the stress field of a dislocation near the crack tip.

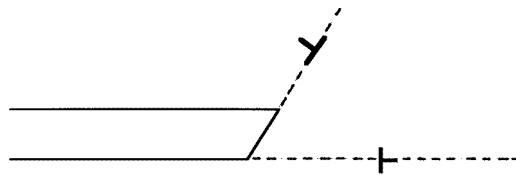


**Figure 9.** Dislocation orientations applied to the finite element mesh.

#### 4.1. Dislocation results

The dislocation loading data is presented in the following order: the stresses calculated for a dislocation along the  $60^\circ$  slip plane, and then the stresses calculated for a dislocation along the  $0^\circ$  crack front. Within the two groups, the radial stresses along the  $0^\circ$  crack front and along the  $60^\circ$  slip plane are presented first. Then, the hoop stresses for the two different directions and finally the shears are given.

The distances from the crack tip or  $60^\circ$  corner,  $r$ , have been normalized by the blunting height,  $h$ . The stress values have been normalized by  $\mu b/h(1 - \nu)$ . Each plot contains the designated stress component for five different dislocation positions. The dislocation positions,  $s$ , are normalized by the burgers vector,  $b$ . For the dislocation along the  $60^\circ$  slip plane plots, the  $s = 1$  refers to the dislocation position that is one burgers vector from the  $60^\circ$  crack corner. Otherwise, the dislocation positions are taken as distances from the  $0^\circ$  crack tip. For the dislocation along the  $0^\circ$  crack front, all distances are measured from the  $0^\circ$  crack tip. Lines connecting the data points are shown in lieu of displaying all the individual data points in order to make the plots more legible.

Figure 10(a) shows the radial stress along the  $0^\circ$  line for a dislocation along the  $60^\circ$  slip plane. Stress fields were calculated for dislocation positions of approximately 77, 52, 26, and 14 burgers vectors from the  $0^\circ$  crack tip, and one burgers vector from the  $60^\circ$  blunted crack corner. By following the curves in figure 10(a), it can be seen that the radial stress

increases as the dislocation moves closer to the 60° crack corner. When the dislocation is very close to the corner, and is about to contribute another row of atoms to the height of the blunted notch, the stress values quickly converge to those of a dislocation at a great distance from the 60° crack corner.

Another plot of interest for a dislocation along the 60° slip plane is the shear stress along the 60° line as shown in figure 10(f). In this plot it is easy to follow the movement of the dislocation because of the stress singularity that results at the dislocation position. Once, again, the influence of the crack is noticed as the dislocation moves closer to the crack corner, but when the dislocation is about to reach the crack corner, the influence of the crack corner on the stress field is quickly diminished.

Figure 11(c) shows the hoop stress along the 0° line for a dislocation along the 0° crack front. Stress fields were calculated for dislocation positions of approximately 77, 52, 26, 13 and one burgers vector from the 0° crack tip. As in figure 10(f), it is easy to follow the movement of the dislocation because of the stress singularity that results at the dislocation position. As expected, the hoop stresses are positive (tensile) behind the dislocation, and negative (compressive) ahead of the dislocation.

#### 4.2. Sharp crack comparison

In order to check the validity of the stress fields of the blunted crack tip in the presence of a dislocation, a comparison can be made with the stress fields of a sharp crack tip in the presence of a dislocation [14]. The stress fields of the two crack tips should converge as the distance from the crack tip increases. The complex potentials for a dislocation ahead of a sharp crack are given by the following formulae

$$\phi'(z) = -\frac{A}{\sqrt{z}} \left\{ \frac{1}{\sqrt{z} + \sqrt{s}} + \frac{1}{\sqrt{z} + \sqrt{\bar{s}}} \right\} + \frac{\bar{A}}{2\sqrt{z\bar{s}}} \frac{(s - \bar{s})}{(\sqrt{z} + \sqrt{\bar{s}})^2} \quad (3a)$$

$$\omega'(z) = -\frac{\bar{A}}{\sqrt{z}} \left\{ \frac{1}{\sqrt{z} + \sqrt{s}} + \frac{1}{\sqrt{z} + \sqrt{\bar{s}}} \right\} - \frac{A}{2\sqrt{z\bar{s}}} \frac{(s - \bar{s})}{(\sqrt{z} + \sqrt{\bar{s}})^2} \quad (3b)$$

where

$$A \equiv \frac{\mu(b_1 + ib_2)}{8\pi i(1 - \nu)} \quad z = r e^{i\theta} \quad s = t e^{i\alpha} = \text{dislocation position.} \quad (3c)$$

Knowing the complex potentials, the polar stress components can be calculated:

$$\sigma_{rr} + \sigma_{\theta\theta} = 4 \operatorname{Re}\{\phi'(z)\} \quad (4a)$$

$$\sigma_{\theta\theta} - \sigma_{rr} + 2i\sigma_{r\theta} = 2[\bar{z}\phi''(z) + \omega'(z) - z\phi''(z) - \phi'(z)] e^{2i\theta}. \quad (4b)$$

The calculations performed on the complex potentials are discussed in detail in appendix B. Figure 12 compares the stress values obtained from the finite element model and the values obtained from the complex potentials of a sharp crack with a dislocation ahead of it. These values do not include the superposition of the dislocation in a continuum. The sharp and blunt crack results are comparable near the 0° crack tip. The two results diverge in the vicinity of the 60° crack corner and then converge as the distance from the crack corner increases.

## 5. Concluding remarks

Solutions of the stresses near the blunted crack tip have been obtained for two types of loading. In both cases—mode I loading and near tip dislocation loading—an analytical

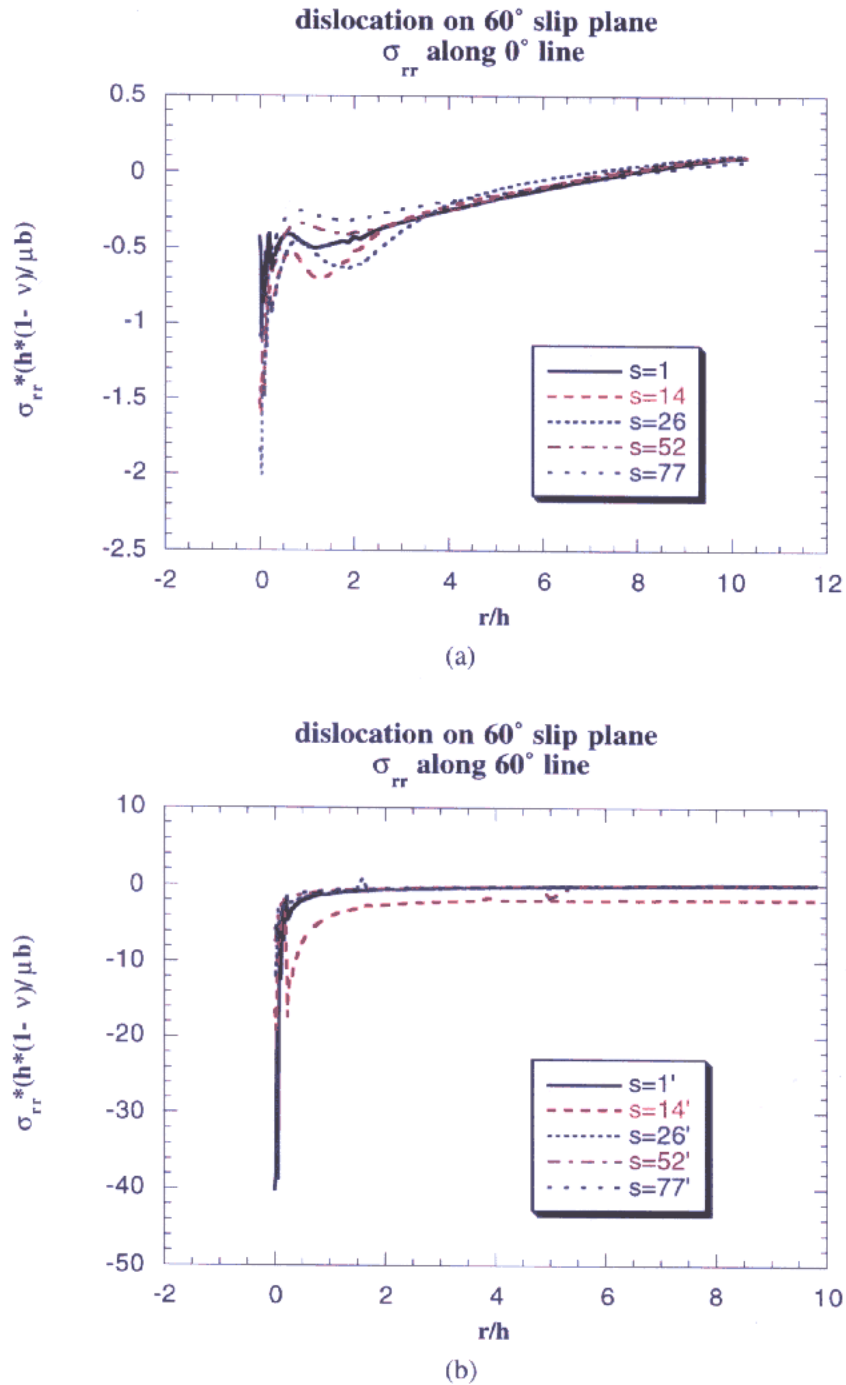


**Figure 10.** Results of the stress fields due to a dislocation along the 60° slip plane where  $s$  is the distance between the dislocation and the crack front normalized by the burgers vector. (a) The radial stress on the 0° crack front, (b) the radial stress on the 60° slip plane, (c) the hoop stress on the 0° crack front, (d) the hoop stress on the 60° slip plane, (e) the shear stress on the 0° crack front, and (f) the shear stress on the 60° slip plane.

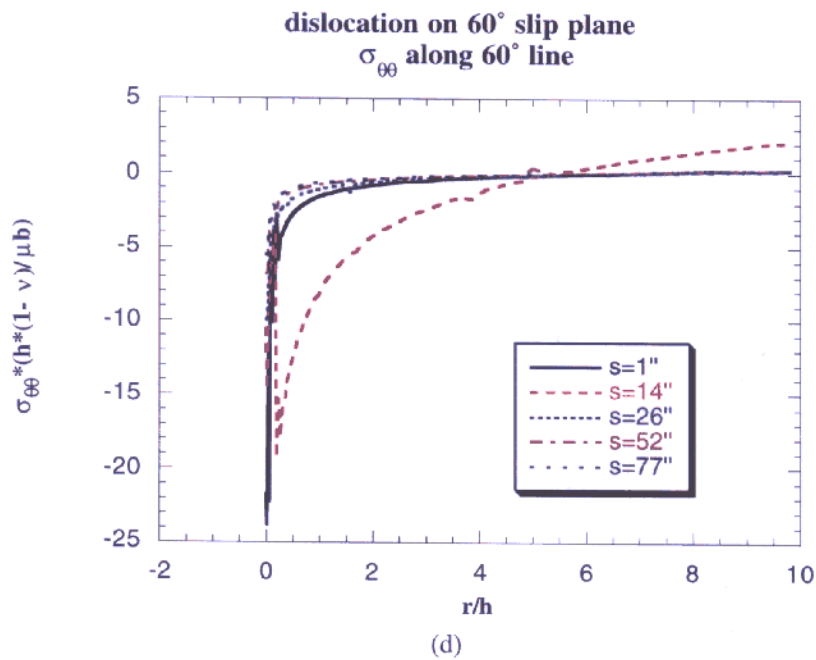
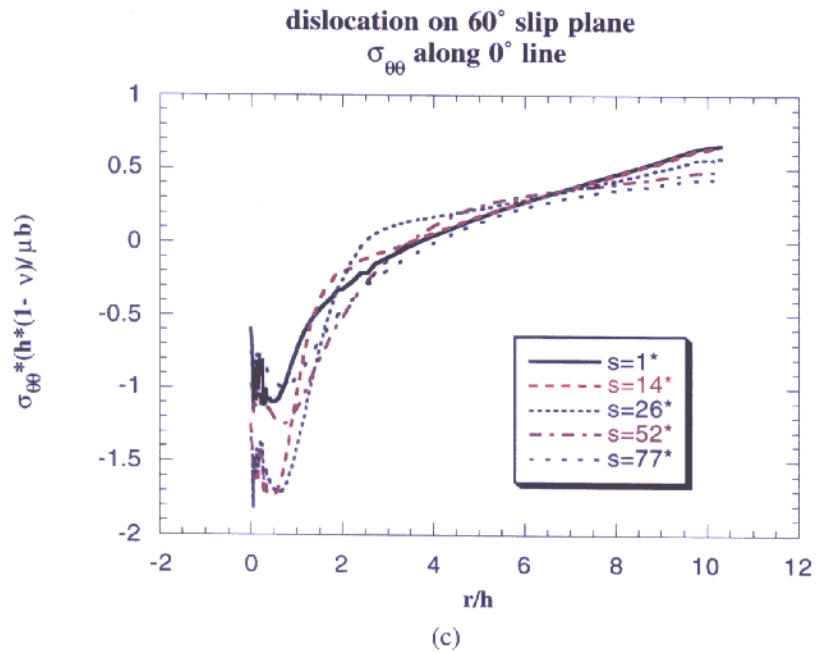


**Figure 10.** (Continued)

comparison of a similar configuration has been made and resulted in good agreement. Since these solutions are purely elastic it is important to point out that, in regions that predict

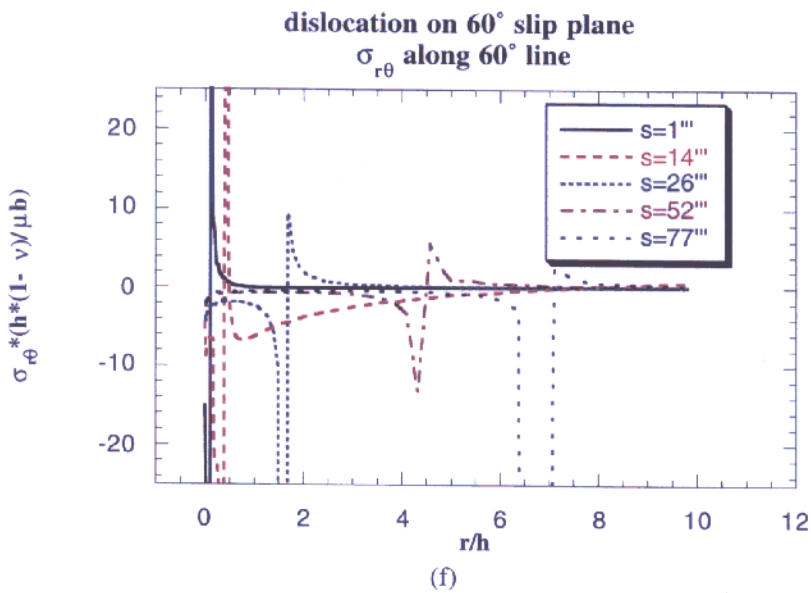
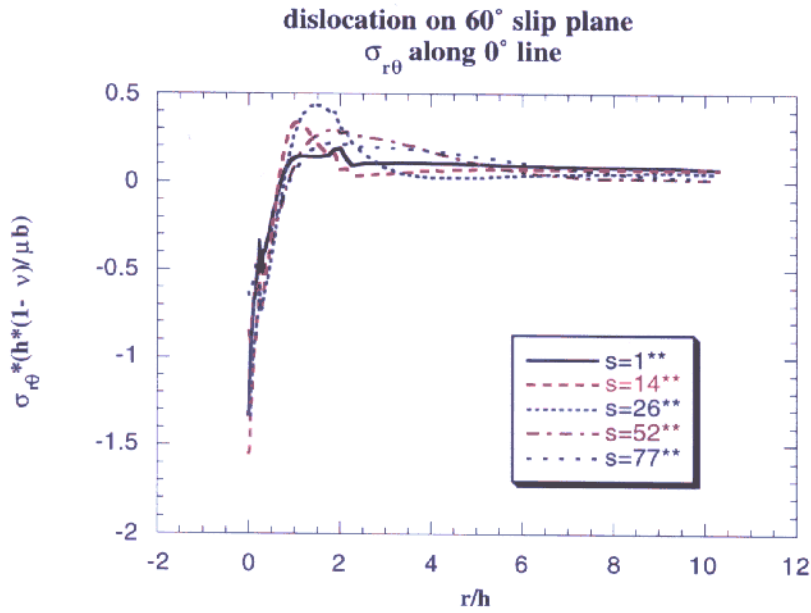


**Figure 10.** (Continued)

high stress, there will actually be nonlinear phenomena such as dislocation formation and/or significant atomic separation. This limit of applicability is analogous to that of the normal elastic crack solution. Nonlinear phenomena will be considered in later work. The validity of the solutions are also compromised near the outer boundaries where assumptions are made about being far from the crack or that the crack lies in an infinite solid. Fortunately,

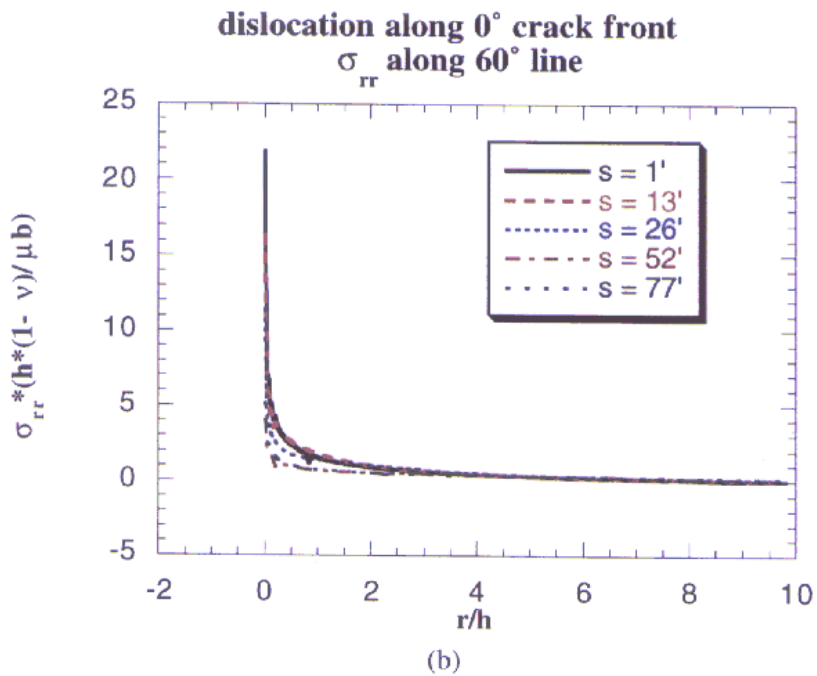
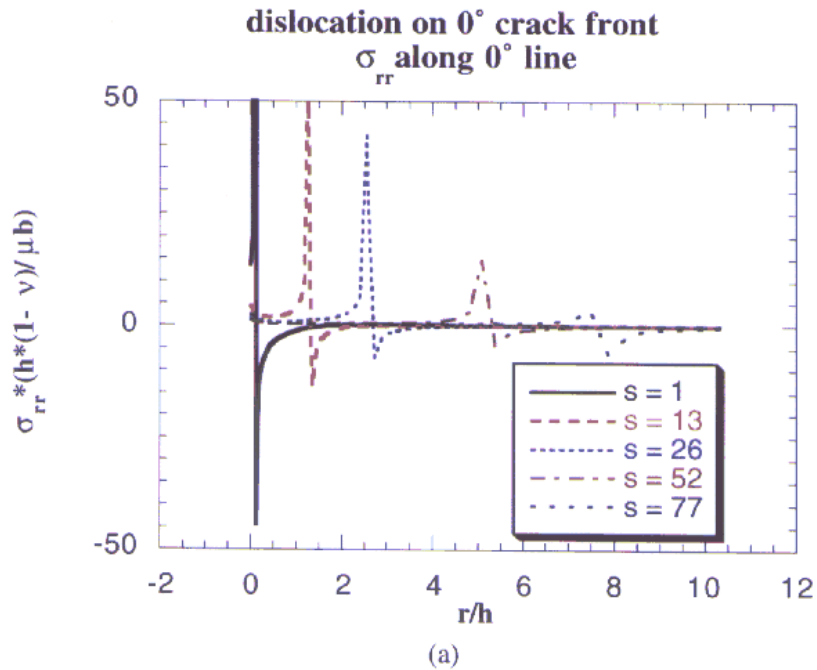


**Figure 11.** Results of the stress fields due to a dislocation along the 0° crack front where  $s$  is the distance between the dislocation and the crack front normalized by the burgers vector. (a) Radial stress on the 0° crack front, (b) radial stress on the 60° slip plane, (c) hoop stress on the 0° crack front, (d) hoop stress on the 60° slip plane, (e) shear stress on the 0° crack front, and (f) shear stress on the 60° slip plane.

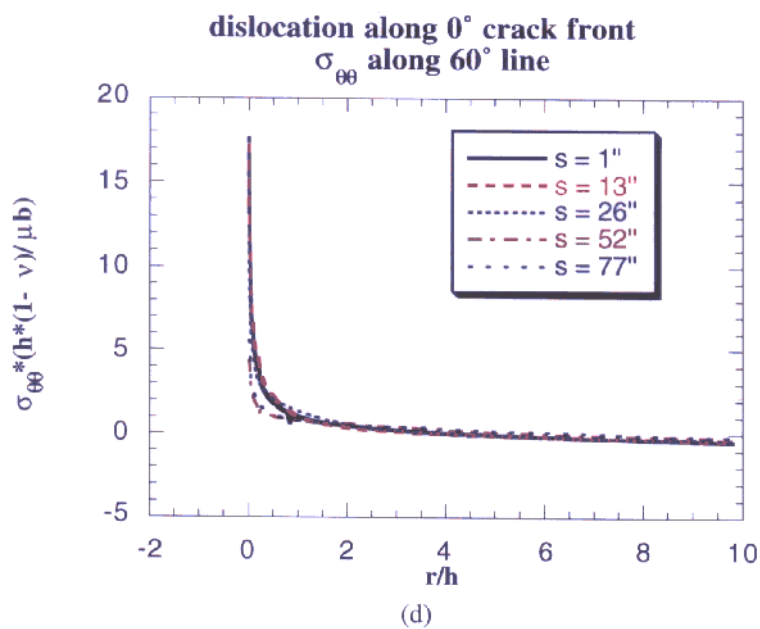
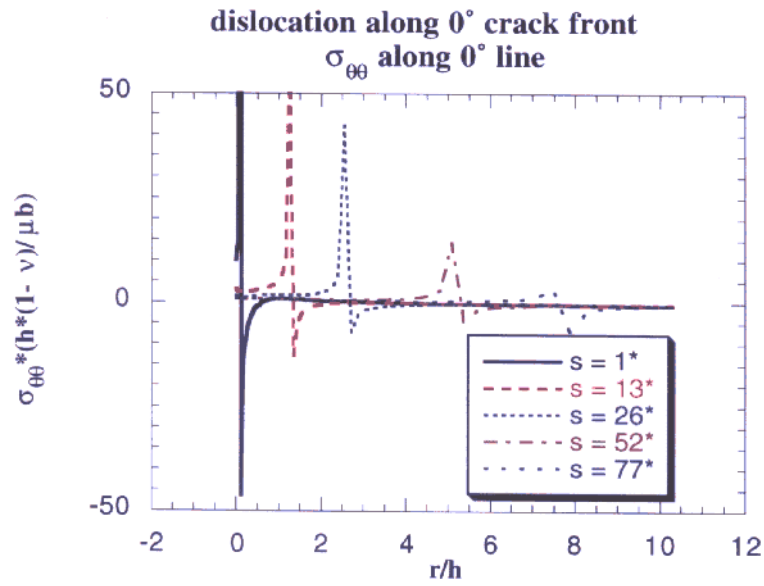


**Figure 11.** (Continued)

we are interested in the stresses relatively close to the crack tip. Perhaps the most important observation is that the stress fields can significantly differ from those obtained for a perfectly sharp crack tip, especially near the tip. This difference between the sharp and blunt crack stress fields may explain some of the disparity between earlier continuum models of ductile

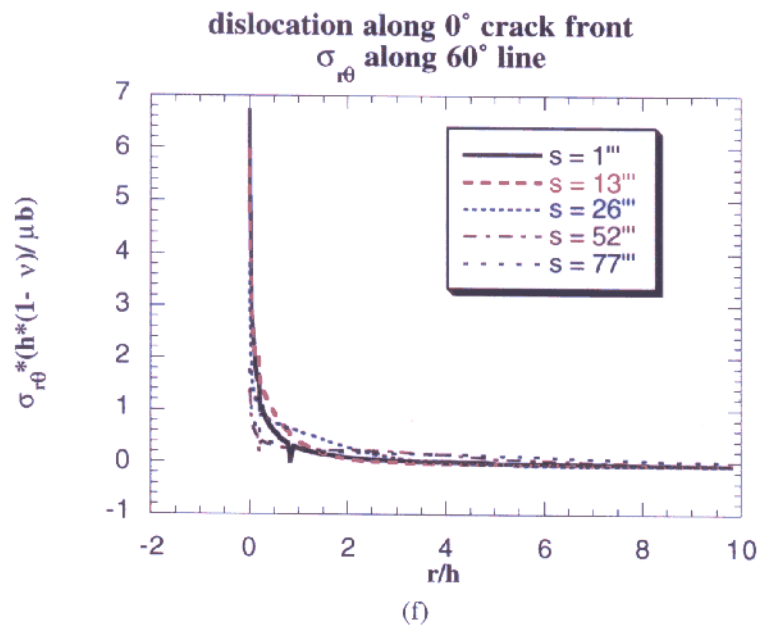
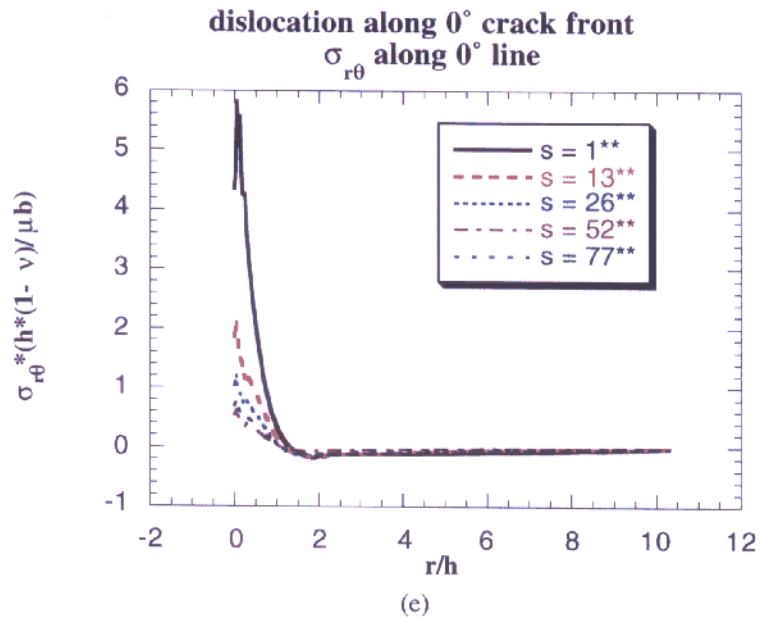


**Figure 11.** (Continued)

versus brittle behavior and more recent atomistic models.

Suppose that a slip plane intersects the crack plane and that the intersection line is also the crack front, and that the slip plane makes an angle  $\theta$  with the crack plane. Assume that the crack tip is loaded in mode I, and that the crack remains stationary. Continuum theories based on the Peierls–Nabarro model [2, 6, 15] assume that the stress concentration

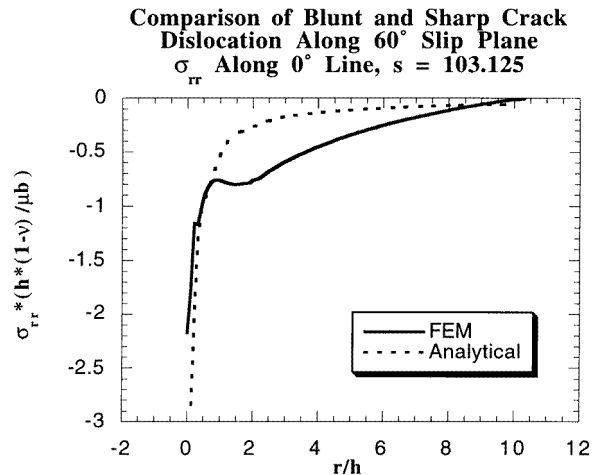


**Figure 12.** Comparison of finite element results for the presence of a dislocation near a blunted crack tip with the sharp crack asymptotic stress field solved using complex potentials. For this case, the dislocation was positioned along the slip plane about 26 burgers vectors from the crack tip or 2.6 times the crack height,  $h$ .

near the crack tip is relieved by an emergent zone of displacement discontinuity across the slip plane, i.e. an incipient dislocation. The incipient profile  $\delta(s)$  can be regarded as a continuous distribution of an individual dislocation at location  $s$  of an infinitesimal burgers vector. Integral equations that impose a force balance at a material point  $r$  along the slip plane may be written in the form

$$\sigma[\delta(r)] = \sigma_0(r) + \int_0^\infty g(r, s, \theta) \left[ -\frac{d\delta(s)}{ds} ds \right] \quad (5)$$

where  $\sigma_0(r)$  is the unrelaxed stress, as provided in section 3 of this paper, and  $g(r, s, \theta)$  corresponds to the stress due to one infinitesimal dislocation, as provided in section 4. The left-hand side,  $\sigma[\delta]$ , is the lattice restoring shear and tension stress against the displacement discontinuities with various forms discussed in [2, 15] and references therein.

In future work, the finite element results presented in this paper will be integrated into this continuum framework in order to understand the competition between crack growth and dislocation nucleation for a crack that may atomically blunt during dislocation formation. The above scheme may be invoked in any number of possible slip planes simultaneously, as well as the crack propagation plane. The results from the respective loadings of the finite element model will make it possible to compare the relative likelihood of crack reinitiation versus dislocation nucleation. Ultimately, these elastic solutions will be used to assess the role of finite crack blunting in the competition between dislocation nucleation and crack reinitiation, and will attenuate certain discrepancies between continuum and atomistic models of this phenomenon.

### Acknowledgments

This work was supported by the Academic Senate Committee on Research of the University of California, Santa Barbara, the LLNL Seaborg Institute of Transactinium Science, and National Science Foundation under award No CMS-9634647. Discussions with

Drs Jakob Schiøtz, Anders Carlsson, Robb Thomson, Sinisa Mesarovic, Don Lipkin, and Alexei Romanov proved most insightful during the course of this work.

### Appendix A. Williams solution for mode I stress singularities of wedge-shaped cracks

The Airy stress function for mode I symmetry can be written in general form:

$$\Phi_a = r^{\lambda+2}[A \cos \lambda\theta + B \cos(\lambda + 2)\theta].$$

The stress components can be found from the Airy stress function as follows [16]:

$$\sigma_{rr} = \frac{1}{r^2} \frac{\partial^2 \Phi_a}{\partial \theta^2} + \frac{1}{r} \frac{\partial \Phi_a}{\partial r} = -(\lambda + 1)r^\lambda [A(\lambda - 2) \cos \lambda + B(\lambda + 2) \cos(\lambda + 2)\theta]$$

$$\sigma_{\theta\theta} = \frac{\partial^2 \Phi_a}{\partial r^2} = (\lambda + 2)(\lambda + 1)r^\lambda [A \cos \lambda\theta + B \cos(\lambda + 2)\theta]$$

$$\sigma_{r\theta} = -\frac{1}{r} \frac{\partial^2 \Phi_a}{\partial r \partial \theta} + \frac{1}{r^2} \frac{\partial \Phi_a}{\partial \theta} = (\lambda + 1)r^\lambda [A\lambda \sin \lambda\theta + B(\lambda + 2) \sin(\lambda + 2)\theta].$$

Enforcing a traction free boundary condition at  $\theta = \pi \pm \beta/2$  for a wedge like that in figure 13 gives

$$\sigma_{\theta\theta} = \sigma_{r\theta} = 0.$$

Equating  $\sigma_{\theta\theta}$  and  $\sigma_{r\theta}$  at  $\theta = \pi - \beta/2$  results in

$$\lambda \tan \left( \lambda\pi - \lambda \frac{\beta}{2} \right) = (\lambda + 2) \tan \left( \lambda\pi - \lambda \frac{\beta}{2} - \beta \right).$$

Figure 14 plots the real part of  $\lambda$  against  $\beta$ , the angle of the crack. From this plot we can see that for  $\beta = 120^\circ$ ,  $\lambda = -0.3843$ , and for  $\beta = 60^\circ$ ,  $\lambda = -0.4875$ .

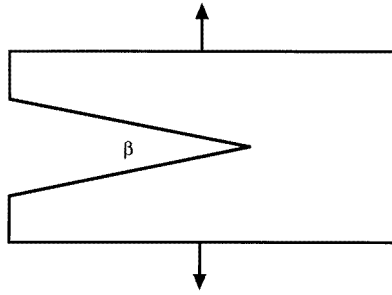


**Figure 13.** Wedge of angle  $\beta$  under mode I loading. Configuration for development in appendix A.

### Appendix B. Complex potentials for a dislocation ahead of a crack

In order to check the validity of the stress fields of the blunted crack tip in the presence of a dislocation, a comparison can be made to the stress fields of a sharp crack tip in the presence of a dislocation [14]. The stress fields of the two crack tips should converge as

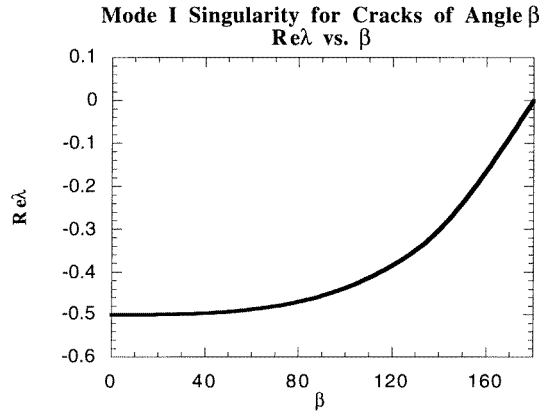


**Figure 14.** Mode I singularity for a crack of angle  $\beta$ .

the distance from the crack tip increases. The complex potentials for a dislocation ahead of a crack are given by the following formulae

$$\phi'(z) = -\frac{A}{\sqrt{z}} \left\{ \frac{1}{\sqrt{z} + \sqrt{s}} + \frac{1}{\sqrt{z} + \sqrt{\bar{s}}} \right\} + \frac{\bar{A}}{2\sqrt{z\bar{s}}} \frac{(s - \bar{s})}{(\sqrt{z} + \sqrt{\bar{s}})^2}$$

$$\omega'(z) = -\frac{\bar{A}}{\sqrt{z}} \left\{ \frac{1}{\sqrt{z} + \sqrt{s}} + \frac{1}{\sqrt{z} + \sqrt{\bar{s}}} \right\} - \frac{A}{2\sqrt{z\bar{s}}} \frac{(s - \bar{s})}{(\sqrt{z} + \sqrt{\bar{s}})^2}$$

where

$$A \equiv \frac{\mu(b_1 + ib_2)}{8\pi i(1 - \nu)} = C(b_2 - ib_2) \quad z = r e^{i\theta} \quad s = t e^{i\alpha} = \text{dislocation position.}$$

Knowing the complex potentials, the polar stress components can be calculated as

$$\sigma_{rr} + \sigma_{\theta\theta} = 4 \operatorname{Re}\{\phi'(z)\}$$

$$\sigma_{\theta\theta} - \sigma_{rr} + 2i\sigma_{r\theta} = 2[\bar{z}\phi''(z) + \omega'(z) - z\phi''(z) - \phi'(z)] e^{2i\theta}.$$

For this check, we wish to find  $\sigma_{rr}$  along the  $0^\circ$  line for a dislocation positioned along the  $60^\circ$  slip plane. Thus,  $\theta = 0$ ,  $z = x$ , and  $s = t e^{i\pi/3}$ .

Simplifying gives

$$\sigma_{\theta\theta} - \sigma_{rr} + 2i\sigma_{r\theta} = 2[\omega'(x) - \phi'(x)] e^{2i\theta}$$

$$\sigma_{\theta\theta} - \sigma_{rr} = \operatorname{Re} \left\{ 2[\omega'(x) - \phi'(x)] e^{2i\pi/3} \right\}.$$

Then

$$\sigma_{rr} = \frac{1}{2} \left( 4 \operatorname{Re}\{\phi'(x)\} - \operatorname{Re} \left\{ 2[\omega'(x) - \phi'(x)] e^{2i\pi/3} \right\} \right).$$

Substituting for  $\phi'(x)$  and  $\omega'(x)$  from the above gives

$$\sigma_{rr} = 2 \operatorname{Re} \left\{ \frac{-C}{\sqrt{x}} (b_2 - ib_1) \left( \frac{1}{\sqrt{x} + \sqrt{s}} + \frac{1}{\sqrt{x} + \sqrt{\bar{s}}} \right) + \frac{C(b_2 - ib_1)}{2\sqrt{x\bar{s}}} \frac{(s - \bar{s})}{(\sqrt{x} + \sqrt{\bar{s}})^2} \right\}$$

$$- \operatorname{Re} \left\{ e^{2i\pi/3} \left[ \frac{C(-ib_1)}{\sqrt{x}} \left( \frac{1}{\sqrt{x} + \sqrt{s}} + \frac{1}{\sqrt{x} + \sqrt{\bar{s}}} \right) - \frac{Cb_2}{\sqrt{x}} (s - \bar{s}) \left( \frac{1}{\sqrt{s}(\sqrt{x} + \sqrt{s})^2} + \frac{1}{\sqrt{\bar{s}}(\sqrt{x} + \sqrt{\bar{s}})^2} \right) \right] \right\}.$$

We can now substitute some of the complex values for the variables. In order to compare the complex potential answers with the finite element calculations, we must choose an unnormalized value of  $s$  that was used in the finite element calculations. Given that the scalar value of  $s$  is  $t = 103.125$ , then

$$\begin{aligned} b_1 &= 3.46 & s_1 &= 51.6 & \text{where } s &= s_1 + is_2 \\ b_2 &= 2 & s_2 &= 89.3. \end{aligned}$$

$\sigma_{rr}$  can now be solved for various values of  $x$ . When  $\sigma_{rr}$  is normalized by  $C$ , the analytical values can be compared to the finite element results. Figure 12 compares the stress values obtained from the finite element model and the values obtained from the complex potentials of a sharp crack with a dislocation ahead of it. These values do not include the superposition of the dislocation in a continuum.

## References

- [1] Rice J R and Thomson R 1974 Ductile versus brittle behavior of crystals *Phil. Mag.* **29** 73
- [2] Xu G, Argon A S and Ortiz M 1995 Nucleation of dislocations from crack tips under mixed modes of loading: implications for brittle against ductile behavior of crystals *Phil. Mag. A* **72** 415
- [3] Schiøtz J, Carlsson A E, Canel L M and Thomson R 1996 Effect of crack blunting on subsequent propagation *Mater. Res. Soc. Symp. Proc.* **409** 95
- [4] Schiøtz J, Canel L M and Carlsson A E 1997 Effects of crack tip geometry on dislocation emission and cleavage: a possible path to enhanced ductility *Phys. Rev. B* **55** 6211
- [5] Williams M L 1952 Stress singularities resulting from various boundary conditions in angular corners of plates in extension *J. Applied Mech.* **19** 526
- [6] Gumbsch P and Beltz G E 1995 On the continuum versus atomistic descriptions of dislocation nucleation and cleavage in nickel *Modelling Simulation Mater. Sci. Eng.* **3** 597
- [7] Gumbsch P 1996 An atomistic study of brittle fracture: towards explicit failure criteria from atomistic modelling *J. Mater. Res.* **10** 2897
- [8] Thomson R 1995 Intrinsic ductility criterion for interfaces in solids *Phys. Rev. B* **52** 7124
- [9] Gann L L 1996 Continuum mechanics of crack tip blunting on the atomic scale: elastic solutions *Thesis* University of California at Santa Barbara
- [10] Barsoum R S 1976 On the use of isoparametric finite elements in linear fracture mechanics *Int. J. Num. Methods Eng.* **10** 25
- [11] Tada H, Paris P C and Irwin G R 1985 Crack-tip stress fields for linear elastic bodies *The Stress Analysis of Cracks Handbook* 2nd edn (St Louis, MO: Paris Production Inc. and Del Research Corporation) p 1.4a
- [12] Hsia K J, Suo Z and Yang W 1994 Cleavage due to dislocation confinement in layered materials *J. Mech. Phys. Solids* **42** 877
- [13] Hirth J P and Lothe J 1968 *Theory of Dislocations* (New York: McGraw-Hill) p 74
- [14] Thomson R 1986 Physics of fracture *Solid State Physics* vol 39, ed H Ehrenreich and D Turnbull (Orlando, FL: Academic) p 31
- [15] Sun Y, Beltz G E and Rice J R 1993 Estimates from atomic models of tension-shear coupling in dislocation nucleation from a crack tip *Mater. Sci. Eng. A* **170** 67
- [16] Timoshenko S P and Goodier J N 1970 Two dimensional problems in polar coordinates *Theory of Elasticity* 3rd edn (New York: McGraw-Hill) p 66